UDC 629 . 11 . 023 : 539 . 43 : 62 - 752

Technical Report

Evaluation of Fatigue and Noise-and-vibration Properties of Automobile Partial Models

Atsushi SETO* Yuichi YOSHIDA
Toyoki YAMAMOTO Shintaro KANOKO

Abstract

Application of high strength steel sheets to automotive bodies requires evaluation technologies of fatigue and noise-and-vibration properties with high accuracy. Automobile partial models were used instead of real bodies for investigation of evaluation methods of those properties. Structural stress concentration parameters gave good estimation of fatigue lives to both of spot-welded and arc-welded models. New analysis methods were proposed for better understanding of vibration phenomena in low- and mid-frequency ranges using bonded models of panel-frame and two panels.

1. Introduction

Efforts have been made to expand the application of high-strength steel sheets to various automotive parts and to develop new automotive steel sheets with higher strength in order to reduce the weight of car bodies without impairing their crashworthiness. When applying high-strength steel sheet to a car body, it is necessary to consider not only crashworthiness but also, for example, the fatigue strength, flexural and torsional rigidity, and vibroacoustic properties that affect car body function.[1-3] It has been shown that the fatigue strength of a base metal improves with increasing tensile strength, while that of a weld joint remains almost constant even when tensile strength is increased.[4, 5] Therefore, the increase in stress applied to a car body due to a reduction in steel sheet thickness causes the fatigue strength of the car body, including the welds, to decline. The flexural and torsional rigidity and vibroacoustic properties of a car body depend largely on the thickness and Young's modulus of the steel sheet used. These properties also deteriorate when the steel sheet thickness is reduced. Therefore, when applying higher strength steel sheet to a car body, it is necessary to predict accurately the fatigue properties, rigidity, and vibroacoustic properties of the car body; furthermore, it is necessary to consider a suitable car body structure and fabrication process at the design stage to compensate for the deterioration of car body functions.

Previously, Nippon Steel Corporation has continuously improved the properties of the steel sheets it manufactures.[6] Upon recognizing that development of technology to predict the fatigue life and vibroacoustic properties of car bodies is also important, the company began to study techniques to evaluate these factors using models of car body members. This report presents concrete examples of evaluation of such properties.

2. Evaluation of Fatigue Properties of Members

2.1 Background

Many of the members of a car body that must be mass produced are made of pieces of steel sheet joined together by, for example, spot or arc welding. These welds are subject to stress concentrations and tend to become weak spots in terms of fatigue strength. Therefore, in designing the structure of a specific member to maintain or enhance its fatigue strength, it is important to accurately predict and evaluate the fatigue strength of the welded parts of the member. In recent years, in order to implement a simple and accurate fatigue design at the stage of car body design, durability of vehicles has commonly been evaluated by CAE using a fatigue analysis program that is freely available. Here, we describe the results of a fatigue test of automobile partial models and the results of prediction of the fatigue life of those partial models conducted using a fatigue analysis program that is widely available. In addition, we verify and discuss

* Chief Researcher, Dr.Eng., Forming Technologies R&D Center, Steel Research Laboratories
20-1 Shintomi, Futtsu, Chiba 293-8511

the prediction results.

2.2 Evaluation of fatigue life of spot-welded members

2.2.1 Prediction techniques

Many studies have been conducted to evaluate the fatigue strength of spot welds. Several researchers have evaluated the fatigue life of spot welds under multiaxial loading using the nominal structural stress (maximum principal stress) of spot welds derived from the elastic deformation theory of plates as the evaluation parameter.[7, 8] These studies reported that it is possible to use the nominal structural stress to evaluate the fatigue life of almost all spot welds, regardless of loading mode and sheet thickness. Other researchers predicted the fatigue limit of spot-welded joints of 980 MPa-class steel sheet using the fracture criterion from a mixed mode crack with a focus on the process of propagation of cracks at the nugget ends.[9] Other researchers performed FEM calculations to study the effects of sheet thickness change, prestrain, and residual stress on the fatigue properties of formed steel sheets for actual car body parts.[10] Here, we use the commercial fatigue analysis program, FE-Fatigue (which has a built-in fatigue life calculation algorithm based on nominal structural stress), to discuss the validity of this evaluation technique on the basis of fatigue data from spot-welded members of mild steel that have been published previously.[11]

The nominal structural stress that handles nuggets as point junctions represents the structural stress concentration. It is calculated by applying the theoretical formula of plate elastic deformation to the shared load acting upon the spot weld, the nugget diameter, and the sheet thickness. The shared load acting upon the spot weld is obtained by FEM structural analysis. A spot-weld model consisting of a BAR element or hexahedral solid element and a link element is used. **Fig. 1** illustrates the fatigue test results for simple spot-welded joints, members with hat-shaped cross sections, and T-jointed members with rectangular cross sections, expressed in the form of fatigue life diagrams based on the nominal structural stress. The fatigue test data are distributed over a relatively narrow range, suggesting that, by using the nominal structural stress, it is possible to accurately predict the fatigue life of almost all spot welds regardless of the joint shape, loading mode, and sheet thickness.

2.2.2 Fatigue test of model members and evaluation of their life

As an example of the application of the prediction technique described in the previous subsection, we fabricated a rectangular section member by spot welding a press-formed 590 MPa-class dual-phase high-strength steel sheet of 1.2 mm in thickness and subjected the fabricated member to a fatigue test under cyclic torsional loading to predict the fatigue life of the member. The shape of the specimen member is illustrated in **Fig. 2**. The specimen member that simulates part of the automotive framework changes in cross-sectional size along its length and a bottom plate is spot welded to it. The shaped member was fabricated as follows. First, the steel sheet was press formed under a blank holding force (BHF) of 400 kN. Then, the press-formed steel sheet was assembled into a box-shaped section member by spot welding the flanges to the bottom plate while they were held together by a fixing jig. The spot welding was performed in such a manner that the residual stress due to springback acted upon the spot welds. To judge the fatigue life of the spot welds, strain gauges were attached in the vicinity of the nuggets to obtain the history data of strains; the time when the strain range around the nugget became zero was defined as the nugget's external crack propagation life.[8]

In the fatigue life calculations, FEM elastic analysis of the member being assembled and the member under torsional loading were conducted, taking into account the influence of springbacks. In addition, the technique to evaluate the fatigue life of spot welds on the basis of nominal structural stress was used. In the elastic analysis of the member during assembly, the stress distribution in the member at the press bottom dead center (obtained by a forming analysis) was used as the driving force to determine the shared load acting on the spot weld and calculate the nominal structural stress.

General-purpose solvers (PAM-STAMP, ABAQUS) were used for the FEM calculations. In the forming analysis, Hill's anisotropic yield function and Swift's model were used as the material model and hardening rule, respectively. The parameter for the equation of Hill was determined by the r-value of specimen materials (r_0 = 0.778, r_{45} = 0.795, r_{90} = 1.025), and F = 1,032 MPa, ε_0 = 0.0003, and n = 0.191 were used as the parameters for the equation of Swift. The nominal structural stress acting on the spot weld owing to springback was set as the average stress for the purpose of fatigue life calculations[12] and the nominal structural stress arising from torsional loading was handled as a variable stress component. The standard SN data of FE-Fatigue for mild steel was converted to the SN data for 590 MPa steel sheet for the reference SN diagram of spot welding used in the fatigue life calculations. The average stress sensitivity used was 0.1.

Fig. 3 shows the maximum principal stress distribution in the specimen base metal obtained by FEM elastic analysis under a torsional load of 85 Nm. The weld in which a fatigue crack occurred was the spot weld of the stretch-flanged part at the center of the

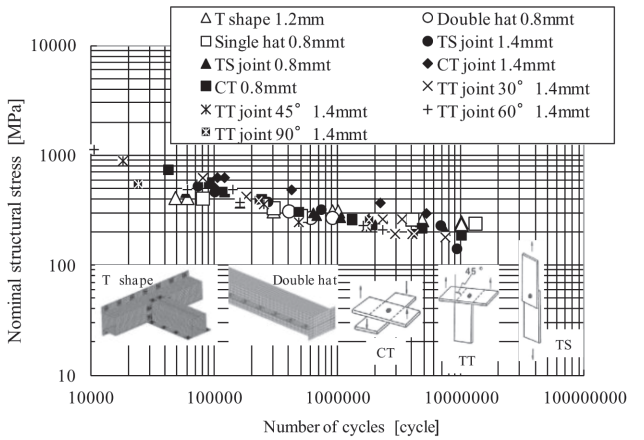

Fig. 1 Comparison between predicted and experimental results on spot welded joints

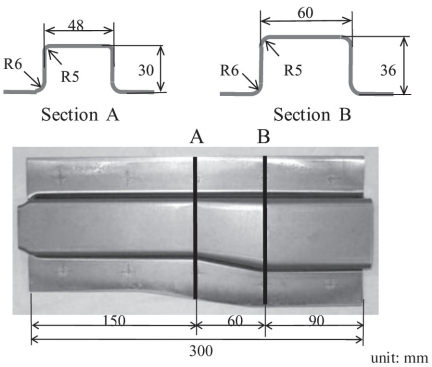

Fig. 2 Spot welded rectangular-shaped section member

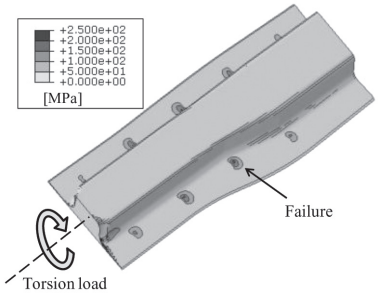

Fig. 3 Maximum principal stress distribution on the base metal

Table 1 Comparison between predicted and experimental results on spot welded rectangular-shaped section member

Torsion load (Nm)	Experiment (cycle)	Prediction (cycle)
85	294,000	164,000
60	964,000	988,000

member. It coincided with the position subjected to a high stress, as indicated by the analysis results. **Table 1** shows the fatigue test results and fatigue life prediction results under different cyclic torsional loads. The predicted fatigue life under a torsional load of 60 Nm almost coincides with the experimental results. Thus, we could obtain valid calculation results by applying the prediction technique that assumes the residual stress caused by springback as the average stress and uses the nominal structural stress as a parameter for fatigue evaluation.

2.3 Evaluation of fatigue life of arc-welded members

2.3.1 Prediction techniques

Arc-welded members are susceptible to fatigue cracking at the weld toes or roots. Therefore, the hot spot stress in the vicinity of a weld toe is often used as an evaluation parameter for fatigue life prediction.[13] In fact, several different evaluation techniques have been proposed. One of these assumes the weld toe to be a notch and uses the size of the cyclic small-scale yield region, the ω*-value, in the vicinity of the notch as an evaluation parameter.[14] Another technique models a weld bead using BAR elements and obtains the nominal structural stress to evaluate the fatigue life.[15] Here, with the focus on fatigue cracking that occurs at the weld toe, we studied the technique that models a weld using shell elements and uses the structural stress (maximum principal stress) that occurs at the node of the weld toe as the evaluation parameter.[16]

Figs. 4 and **5** illustrate the shapes of arc-welded lap joints[17] and a T-shaped arc-welded joint[18] and the loading conditions used in the fatigue tests of those joints. Each of the arc-welded members is made from a hot-rolled steel sheet with a tensile strength of 440 MPa and a thickness of 2.3 mm, and each of the weld beads has a weld start point and a weld end point. The T-shaped arc-welded joint is a model member proposed by joint research of the Society of Automotive Engineers of Japan and simulates the joint of a chassis component. To judge the fatigue life, strain gauges were attached in the vicinity of each weld toe to obtain the history data of strains; the crack initiation life was defined as the time by which the strain range had decreased by 20% from initial conditions.[18]

Fig. 6 shows examples of initiation of a fatigue crack. The fatigue crack in the arc-welded lap joint occurred in the vicinity of the

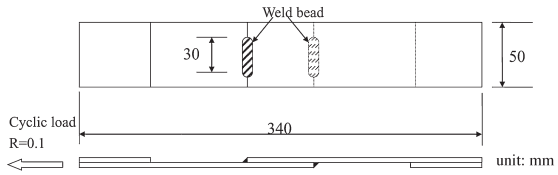

Fig. 4 Schematic representation of arc-welded lap joints with weld start and end point

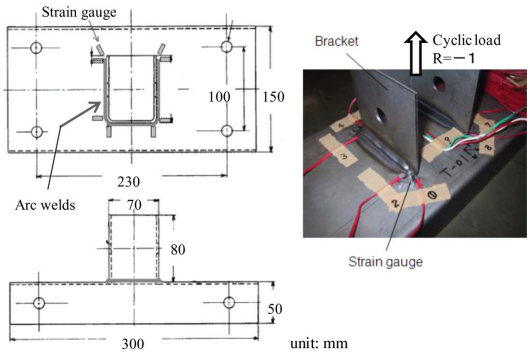

Fig. 5 Schematic of T shape type arc welded joint

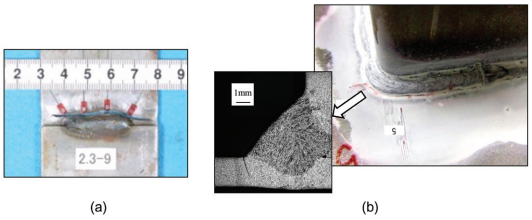

Fig. 6 Fatigue crack initiation of weld part
(a) Arc welded lap joint with weld start and end point, (b) T shape type arc welded joint

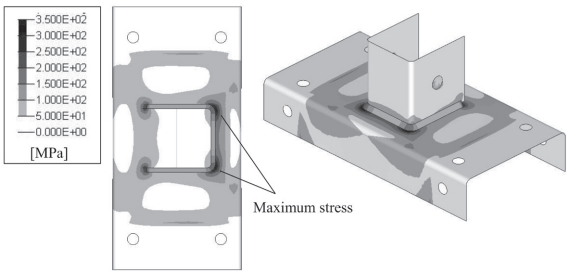

Fig. 7 Equivalent stress distribution on T shape type arc welded joint

weld start point, propagating across the width of the specimen and along the weld toe. And, the fatigue crack in the T-shaped arc-welded joint occurred at the weld toe of the bracket corner and propagated in the thickness direction. **Fig. 7** shows the equivalent stress distribution in the T-shaped arc-welded joint under a 2.5 kN load, obtained by FEM analysis. The part in the analysis result showing the maximum stress coincides with the part in which a fatigue crack occurred.

Fig. 8 presents fatigue life diagrams in which the fatigue test results of each of the joints are summarized in terms of the structural

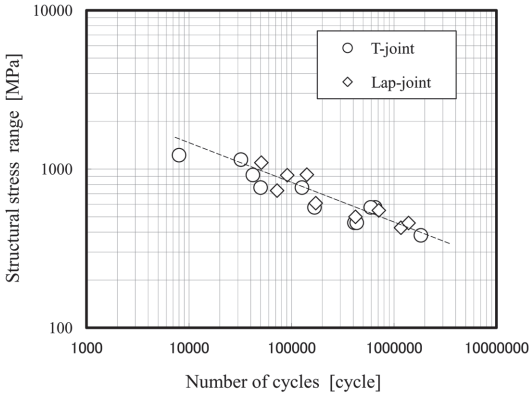

Fig. 8 SN diagram on T shape type joints and lap joints

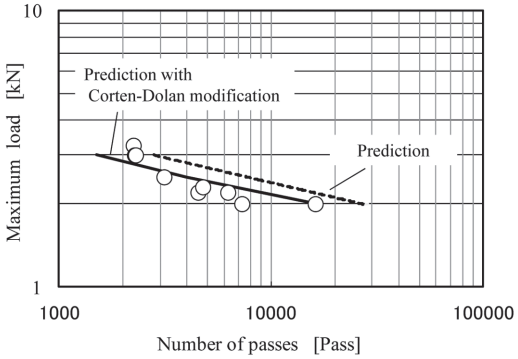

Fig. 10 Comparison between predicted and experimental results on T-shape joint under variable amplitude loading

weld stresses calculated by FEM analysis. The lap joint and T-shaped welded joint exhibit almost the same fatigue strength, and the fatigue test data are distributed over a comparatively narrow range. This suggests that, by expressing fatigue strengths in terms of structural weld stress, it is possible to evaluate the fatigue life of almost any arc-welded member, regardless of joint shape and loading mode.

2.3.2 Evaluation of fatigue life of welds under variable-amplitude loading

The fatigue load acting upon an actual part seldom exhibits constant amplitude; in many cases, both the amplitude and mean value of the load are variable. Here, as an example of application of the prediction technique described in the preceding subsection, we discuss predicting the fatigue life of a T-shaped welded joint when a variable-amplitude loading is applied vertically to a U–shaped bracket of the joint.[19] The variable-amplitude input loads used in the fatigue test are based on the variation patterns (virtual road surface displacement data)[20] of the JARI standard uneven road profile, which were made public at a meeting of the Fatigue Reliability Committee of the Society of Automotive Engineers of Japan. **Fig. 9** shows the time-serial waveform of a variation pattern converted into a normalized waveform by the maximum displacement. A single variation pattern has 531 cycles of variation. Each of the variable-amplitude input loads was set by multiplying the normalized amplitude variation by the prescribed load value.

For fatigue life prediction, the fatigue life diagram shown in Fig. 8 was used as the reference SN data and the cumulative damage rule was used. Specifically, on the basis of the variable-amplitude loads applied in the fatigue test, we calculated the variable stress waveform of the weld from the FEM analysis results, obtained its stress frequency distribution by counting the cycles using the rainflow method, and estimated the fatigue life of the weld in accordance with the modified Miner's rule. In the above fatigue life calculation process, FE-Fatigue—a fatigue analysis program that is widely available—was used.

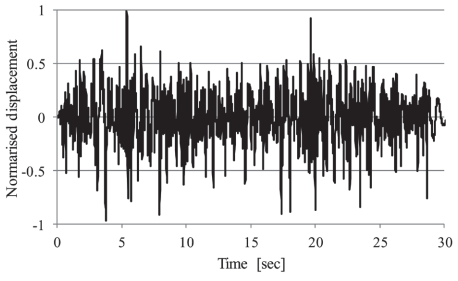

Fig. 9 Variable amplitude data

Fig. 10 displays the results of the fatigue testing and experimentation summarized in terms of the maximum values of variable-amplitude loads. The horizontal axis represents the number of times (number of passes) the variable-amplitude load pattern was applied until the occurrence of a crack in the weld. In the figure, the broken line represents the predicted fatigue life obtained by the procedure described above. The prediction somewhat overestimated the experimental result. The modified Miner's rule calculates the degree of fatigue damage regardless of either the load interaction effect or the sequence of loading. Therefore, depending on the service load waveform, a fatigue failure does not always occur when the degree of fatigue damage is 1. To allow for such a case, a fatigue life prediction method in which the reference SN data itself is modified has been proposed.[21] Under a service load that is subject to frequent changes in stress amplitude and mean stress, the degree of damage caused by a low-level stress near the fatigue limit tends to become larger than when the stress amplitude is constant because of the influence of a high-level stress load. The Corten–Dolan method takes this phenomenon into consideration.

The variable-amplitude load that was used in the fatigue test in the present study was subject to relatively frequent changes of amplitude. Therefore, we recalculated the fatigue life using the Corten-Dolan method. The recommended value of modification coefficient β is between 0.7 and 0.95. In the present estimation, β was assumed to be 0.7 to allow for a large degree of modification and an evaluation on the safe side. In Fig. 10, the solid line represents the recalculated fatigue life. The predicted values after modification of the reference SN reproduce the experimental values relatively well; any differences are considered to be due in part to the load interaction effect.

2.4 Summary

(1) By using the nominal structural stress or some other appropriate parameter that represents the structural stress concentration in a welded member, it should be possible to evaluate the fatigue life of the welded member almost universally, regardless of joint shape and loading mode.

(2) We estimated the fatigue life of a spot-welded member with a rectangular cross section, taking into consideration the influence of its residual stress. The results obtained were considered acceptable. In addition, we predicted the fatigue life of a T-

shaped welded joint under variable-amplitude loading. Using cumulative damage evaluation based on the modified Miner's rule and modification of the reference SN, we were able to reproduce the experimental results well.

3. Evaluation of Vibroacoustic Properties of Parts

3.1 Background

In designing a vehicle body structure, it is common practice to first meet the requirements for crashworthiness and then provide the vehicle body structure panels with damping sheets and sound insulators to reduce vibration and noise. However, the addition to features such as dampers tends to increase vehicle body structure weight significantly. Therefore, it is necessary to predict the sound level in the vehicle even when considering ways to meet requirements for crashworthiness in the early stages of structural design.

With a deepening understanding of vibroacoustic phenomena, various modeling techniques appropriate for the specific frequencies under consideration have come to be used to predict the sound level.

For the low-frequency band, a vibroacoustic analysis technique exists that couples the finite element method (FEM) and the boundary element method (BEM). This technique is suitable primarily for solving the problems of wave propagation through structures and applies both to structures and to acoustic spaces as a whole.

To solve high-frequency vibroacoustic issues, methods such as statistical energy analysis (SEA) are used. SEA calculates the energy that is dependent on the number of modes of a given flat plate and space system, which are divided into subsystems to evaluate the wavelength and number of modes. It is applied mainly to problems of wave propagation through spaces. Problems of mid-frequency vibroacoustic involve both structural and spatial propagation ; thus, such problems cannot be analyzed accurately by any one of the above analytical techniques. In recent years, therefore, hybrid methods such as that combining FEM/BEM with SEA on an energy state have been studied.

In this section, we shall describe the analytical techniques that can be used to efficiently address problems of low- and mid-frequency vibroacoustic and discuss measures to reduce the sound levels from steel parts, excluding the high-frequency vibroacoustic properties, which are related primarily to sound absorbers and other acoustic materials.

3.2 Vibroacoustic analysis techniques applicable to low-frequencies

3.2.1 Background to analysis of low-frequency vibrations

For plate-shaped structures such as automobile floor panels, adding ribs to the flat parts has been presented as a method of reducing the flexural vibration. Since this method permits enhancing the structure stiffness without significant weight increases, it can be used in many cases to reduce the vibration level of the structure.[22, 23] However, it causes the vibration to increase in some cases, highlighting the need for a suitable measure that can be used by trial-and-error. In order to deepen our understanding of the vibration phenomenon and reduce the vibration level efficiently, we propose a new analytical technique that is based on numerical calculations using a mass and stiffness matrix obtained from FEM calculations;[24, 25] we also verify the effectiveness of the technique by applying it to study the phenomenon in which the vibration level increases.

3.2.2 Phenomenon in which vibration of panel construction increases

Fig. 11 (a) illustrates a structure composed of a flat panel and a frame, and Fig. 11 (b) shows a structure composed of a ribbed panel and a frame. The panel boundary conditions in both (a) and (b) were assumed to be in a free state. **Fig. 12** illustrates the velocity response

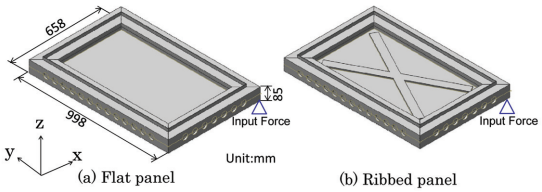

Fig. 11 Panel with frame FE model

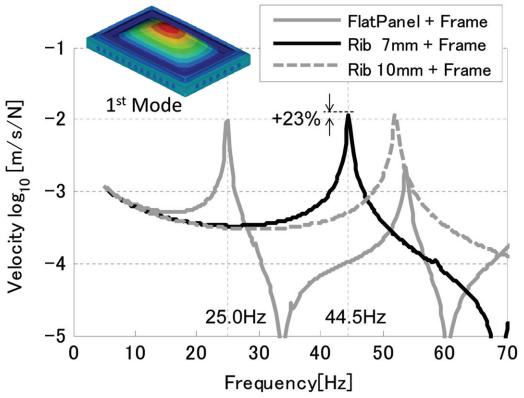

Fig. 12 Velocity response of panel

of each panel around its primary natural frequency. It can be seen that the primary natural frequency increases from 25.0 Hz for the flat panel (a) to 44.5 Hz for the panel with 7-mm-high ribs (b) and that the velocity response increases by about 23% from 0.945×10^{-2} m/s/N (a) to 1.16×10^{-2} m/s/N (b). When the rib height is increased to 10 mm, the velocity response becomes 1.17×10^{-2} m/s/N, as indicated by the chained line in Fig. 12. Thus, an increase in stiffness alone does not lead to a decrease in vibration. Therefore, it may be said that, in order to efficiently reduce the vibration without increasing the weight significantly, it is important to quantitatively evaluate the phenomenon in which the vibration level increases and to implement a structural design based on the evaluation results.

3.2.3 Derivation and application of quantitative evaluation method

In this subsection, we shall explain the method of quantitative evaluation of vibration in which the equation of motion obtained by FEM is divided into two parts—one for the panel and the other for the frame. Each kinetic equation can be expressed as follows. Subscript F denotes the frame component, subscript P the panel component, x the displacement and f the external force vector, respectively.

$$\begin{bmatrix} \mathbf{B}_{FF} & \mathbf{B}_{FP} \\ \mathbf{B}_{PF} & \mathbf{B}_{PP} \end{bmatrix} \begin{Bmatrix} \mathbf{x}_F \\ \mathbf{x}_P \end{Bmatrix} = \begin{Bmatrix} \mathbf{f}_{PF} \\ 0 \end{Bmatrix} \quad (1)$$

In the above formulation, it is assumed that the external force is applied only to the frame. **B** denotes the dynamic stiffness matrix that consists of the stiffness matrix **K**, damping matrix **D**, and mass matrix **M**.

$$\mathbf{B} \equiv \mathbf{K} + j\omega\mathbf{D} - \omega^2\mathbf{M} \quad (2)$$

Solving Equation (1) in terms of the panel component,

$$\mathbf{x}_P = \mathbf{G}_{PP}\mathbf{f}_{PF} \quad (3)$$

where $\mathbf{G}_{PP} \equiv \mathbf{B}_{PP}^{-1}$, $\mathbf{f}_{PF} \equiv -\mathbf{B}_{PF}\mathbf{x}_F$. $\mathbf{G}_{PP}$ denotes the transfer function matrix with the panel boundary fixed completely and $\mathbf{f}_{PF}$ denotes the

force transferred from the frame to the panel. When the evaluated vibration is assumed to be the sum of the weights of specific nodes, it is expressed as the product of weight vector **w** and $\mathbf{x}_P$.

$$x = \mathbf{w}^T\mathbf{x}_P = \mathbf{w}^T\mathbf{G}_{PP}\mathbf{f}_{PF} = \mathbf{g}_P^T\mathbf{f}_{PF} \quad (4)$$

where $\mathbf{g}_P$ denotes the vector that indicates the vibration response of the object, which is used to evaluate the panel boundary input. Since Equation (4) provides the inner product of vectors, it can be converted in terms of the norm product as follows.

$$x = \|\mathbf{g}_P\| \cdot \|\mathbf{f}_{PF}\| \cdot r \quad (5)$$

where r denotes the correlation of vectors.

$$r \equiv \frac{\mathbf{g}_P^T\mathbf{f}_{PF}}{\|\mathbf{g}_P\| \cdot \|\mathbf{f}_{PF}\|} \quad (6)$$

Vibration response x is given precisely as the product of three factors: $\|\mathbf{g}_P\|$, which indicates the vibration level response to the input to the panel boundary (panel transfer function); $\|\mathbf{f}_{PF}\|$, which indicates the amount of force transferred from the frame to the panel; and r (transfer efficiency), which indicates the correlation between the panel transfer function and transferred force. Therefore, in the following subsection, we use the three factors ($\|\mathbf{g}_P\|$, $\|\mathbf{f}_{PF}\|$, and r) that contribute to vibration response x to explain quantitatively the phenomenon in which the vibration level increases.

3.2.4 Understanding the phenomenon using quantitative evaluation

Table 2 summarizes the calculated results of the evaluation indexes $\|\mathbf{g}_P\|$, $\|\mathbf{f}_{PF}\|$, and r for the structures shown in Fig. 11. In the table, each characteristic value of the flat panel with frame (Fig. 11 (a)) is shown for reference (100%). A comparison between (a) and (b) reveals that the addition of ribs reduces both the norm of the transfer function ($\|\mathbf{g}_P\|$) and the norm of the force from the frame to the panel ($\|\mathbf{f}_{PF}\|$) by about 30%. Conversely, the transfer efficiency, r, is increased by about 125%. Thus, by adding ribs to the panel, it became possible to increase panel stiffness and decrease the norms of the transfer function of the panel and the force to the panel. However, the transfer efficiency increased simultaneously, which may have resulted in increasing vibration. Using the technique derived in 3.2.3, it was possible to evaluate quantitatively the correlation between components of a structure.

3.2.5 Optimum design of panel

3.2.5.1 Optimum structural design based on vibration sensitivity

The optimum rib arrangement for a panel was obtained by structural optimization.[26] The conditions for optimization were as follows: the objective function was minimizing the vibration response of the panel surface vibration response by the input force from the frame; the maximum rib height was 5 mm. The optimized panel shape is shown in **Fig. 13**.

Table 2 Result of quantitative evaluation method for panel with frame

	(a) Flat panel with frame	(b) Ribbed panel (7mm)	(c) Optimized panel
1st natural frequency	Base (100%)	178%	160%
Velocity	Base (100%)	123%	67.5%
Norm of transfer function $\|\mathbf{g}_P\|$ (m/s/N)	Base (100%)	30.7%	82.0%
Norm of force $\|\mathbf{f}_{PF}\|$	Base (100%)	32.5%	450%
Correlation r	Base (100%)	124%	18.3%

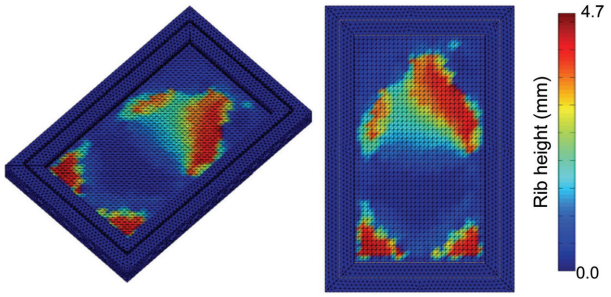

Fig. 13 Contour plot of Rib Pattern

3.2.5.2 Quantitative evaluation of optimization results

For the optimized model shown in Fig. 13, the values of the evaluation indexes $\|\mathbf{g}_P\|$, $\|\mathbf{f}_{PF}\|$, and r were calculated. The calculation results are presented in Table 2 (c). It is clear that the vibration response at the primary natural frequency decreased to about 70% of that of (a). The panel transfer function $\|\mathbf{g}_P\|$ of (c) is about 80% as compared with about 30% of (b). Thus, considering the panel independently, the stiffness of (c) is lower than that of the ribbed panel shown in Fig. 11 (b). The norm of force, $\|\mathbf{f}_{PF}\|$, of (c) is 450%, which is far greater than that of (a), whereas the correlation r (indicating the transfer efficiency of (c)) decreased to about 18% that of (a). From these results, it can be inferred that the vibration response of (c) has decreased. Thus, it is possible to evaluate quantitatively the mechanism by which the vibration increases or decreases using the above technique, and the technique can be considered useful for studying structures.

3.3 Vibration analysis techniques applicable to mid-frequencies

3.3.1 Background to analysis of mid-frequency vibrations

Techniques for analyzing vibrations of low- or high-frequencies have already been established, as described in the preceding section. However, no effective techniques have yet been established for the analysis of vibrations of mid-frequencies, although many different techniques have been proposed. Furthermore, for conventional techniques, it is difficult to judge by experimentation whether the frequency delibetatively is low, middle, or high. Here, as a preliminary evaluation of vibration analysis techniques applicable to mid-frequencies, we propose and discuss a method that defines the mid-frequency band in terms of the ratio between real and imaginary parts of external power.[27]

3.3.2 Proposed method of definition of mid-frequency band

The following equation of motion (7) concerns the relationship between an equation of motion and an equation of SEA power equilibrium. Solving Equation (7) in terms of displacement **x** gives the power balance equation (8).

$$\left((1 + j\eta)\,\mathbf{K} - \omega^2\mathbf{M}\right)\mathbf{x} = \mathbf{f} \quad (7)$$

$$(P_M + P_K) + P_D = P_F \quad (8)$$

where η denotes structural damping; P_M, P_K, and P_D denote the time differentials (powers) of kinetic energy, strain energy, and damping energy, respectively; and P_F denotes the input power. P_M and P_K are purely imaginary numbers, whereas P_D is a real number. Therefore, the following relationships can be obtained by taking the real and imaginary parts of Equation (8).

$$P_D = \mathrm{Re}\,(P_F) \quad (9)$$

$$P_K + P_M = j \cdot \mathrm{Im}\,(P_F) \quad (10)$$

The SEA power equilibrium of a single system is expressed by the following equation, which is equivalent to Equation (10). Therefore, the equation holds true for all frequencies.

$$\omega \eta E_K = \mathrm{Re}\,(P_F) \tag{11}$$

where E_K denotes the strain energy and $P_K = -j\omega E_K$. Therefore, assuming the solution obtained from the equation of motion as the exact one, the equation of motion is equivalent to the equation of SEA power equilibrium when the frequency meets the condition Re (P_F) >> Im (P_F); thus, SEA is applicable.

When determining whether or not SEA is applicable to a specific frequency, the modal overlap factor (MOF)[28] expressed by the following equation has been used as the criterion.

$$\mathrm{MOF} = \omega_C \eta n > 1 \tag{12}$$

where ω_C denotes the center angular frequency of the octave band and n denotes the mode density. Obtaining structural damping η and mode density n experimentally requires considerable labor, and the physical implications of MOF are difficult to ascertain. Therefore, we defined those frequencies that meet the condition Re (P_F) >> Im (P_F) as the frequencies for which SEA is applicable; then, we studied whether it would be possible to explain the high limit of mid-frequency as the boundary of mode analysis and SEA application by the energy ratio between Re (P_F) and Im (P_F) in Equation (13).

$$\theta = \tan^{-1}\left(\mathrm{Im}\,(P_F) / \mathrm{Re}\,(P_F)\right) \tag{13}$$

From the above equation, it can be seen that values of Im (P_F) are smaller for smaller energy ratio θ.

3.3.3 Verification by mode analysis

Using a model composed of two panels joined together in an L-shape, we obtained the value of Re (P_F) in Equation (9) and the value of Im (P_F) in Equation (10). The power was input by rain-on-the-roof excitation,[29] which excites all modes uniformly, and independent complex inputs were assigned to the individual nodes. **Fig. 14** illustrates the values of Re (P_F), Im (P_F), P_D, and $P_K + P_M$. It is clear that Re (P_F) = P_D and $j \times$ Im (P_F) = $P_K + P_M$ hold true. It can also be seen that Re (P_F) becomes greater than Im (P_F) with increasing frequency, indicating that SEA is effective for high frequencies. Conversely, at low frequencies, Re (P_F) and Im (P_F) are almost the same; hence, Im (P_F) cannot be ignored. Thus, it is certain that low frequencies constitute a region in which the mode analysis that focuses on the strain energy and kinetic energy comprising Im (P_F) is effective.

3.3.4 Verification of method of defining mid-frequency band

Fig. 15 shows the Re (P_F) to Im (P_F) ratio θ (left-hand axis) proposed in Equation 13 and the MOF (right-hand axis). In this particular application, values of θ are estimated to be in the range 30 - 45° for MOF > 1 (as shown in Equation (12)) in the mid-frequency band. MOF increases with increasing frequency, while the value of θ remains almost constant. Therefore, we concluded that MOF and θ have different physical meanings. In future, we intend to establish a dependable method of verification and continue our study, with the emphasis on deriving facts experimentally.

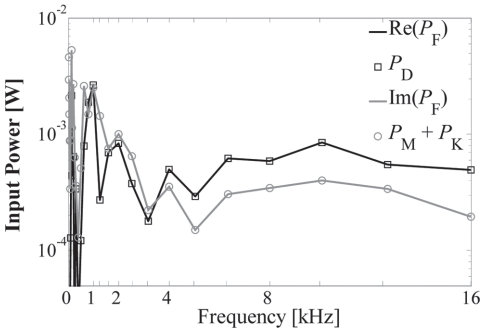

Fig. 14 Frequency dependence of input power

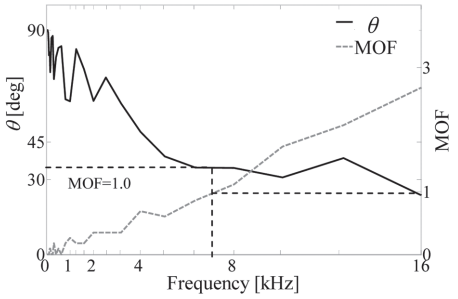

Fig. 15 Relationship between θ and MOF

3.4 Summary

(1) We explained the phenomenon in which the low-frequency vibration level of a panel increases when the panel is provided with ribs. Simultaneously, we defined the correlation r that represents transfer efficiency. In addition, through a quantitative evaluation of the panel optimization results using our proposed technique we were able to clarify how the vibration level could be reduced and prove the validity of the optimization results.

(2) We proposed a new method defining a mid-frequency band based on experimental results, and found that it was possible to omit the preliminary simulation to determine the mode density. In addition, we demonstrated the possibility of making a judgment based on the marginal frequency for the mode analysis that analyzes the deformed shape of the principal component of the object under consideration.

4. Conclusion

Previously described techniques for the evaluation of fatigue and vibroacoustic properties are intended for application primarily to simple partial models. However, with the aid of CAE, any of these techniques can be applied to evaluate properties of models of complicated shape under more severe conditions. In order to expand the application of high-strength steel sheets, we intend to continue improving the precision of the evaluation techniques discussed here.

Acknowledgments

We wish to express our heartfelt thanks to Dr. Nobuyuki Okubo and Dr. Takeshi Toi (professors in the Department of Science and Engineering at Chuo University), and to Dr. Kohei Furuya (assistant professor at Gifu University) for their guidance in our study of technology for evaluating vibroacoustic properties.

References

1) Yamamoto, T.: Nishiyama Memorial Technical Lecture. 74/75, 1981, p. 179
2) Hayashi, K.: Car Body Engineering. 39 (55), 23 (2002)
3) Shibaoka, M.: No. 14-7 Symposium Text of the Society of Automotive Engineers of Japan. 2008, p. 43
4) Takahashi, K. et al.: Collection of Papers (Part 1) of the Japan Society of Mechanical Engineers. 38 (310), 1154 (1972)

5) Watanabe, O. et al.: Outlines of Lectures at National Convention of Japan Welding Society. 52, 256 (1993)
6) Takahashi, M.: Shinnittetsu Giho. (378), 2 (2003)
7) Rupp, A. et al.: SAE Technical Paper Series. 950711, 1 (1995)
8) Kawamoto, J. et al.: No. 06-00 Symposium Text of the Society of Automotive Engineers of Japan. 2000, p. 13
9) Togo, K. et al.: Materials. 58 (7), 627 (2009)
10) Chen, G. et al.: SAE Technical Paper Series. 2002-01-0640, 1 (2002)
11) Mizui, M. et al.: Estimation of Fatigue Life of Spot-Welded Structures of Car Bodies (Results of Joint Research). Society of Automotive Engineers of Japan, 1986, p. 24
12) Nakamura, H. et al.: Fatigue Life Design of Machines. 1st Edition. Yokendo Co., Ltd., Tokyo, 1983, p. 132
13) Japanese Society of Steel Construction: Guidelines on Fatigue Design of Steel Structures and Explanations. 1st Edition. Gihodo Shuppan Co., Ltd., Tokyo, 1993, p. 283
14) Toyama, K. et al.: No. 12-05 Symposium Text of the Society of Automotive Engineers of Japan. 2005, p. 9
15) Kato, K. et al.: Collection of Papers of the Society of Automotive Engineers of Japan. 39 (2), 351 (2008)
16) Fermér, M. et al.: SAE Technical Paper. 982311, 1280 (1998)
17) Seto, A. et al.: Collection of Papers of the Society of Automotive Engineers of Japan. 36 (2), 95 (2005)
18) Akasaki, T. et al.: Collection of Papers of the Society of Automotive Engineers of Japan. 34 (3), 139 (2003)
19) Yoshida, Y. et al.: Collection of Preprints for 2011 Autumn Academic Lecture Meeting of the Society of Automotive Engineers of Japan. 112-11, 2011, p. 9
20) Aoki, T. et al: No. 12-05 Symposium Text of the Society of Automotive Engineers of Japan. 2005, p. 38
21) Yamada, T. et al.: Handbook of Fatigue Design of Metallic Materials. 2nd Edition. Yokendo Co., Ltd., Tokyo, 1981, p. 127
22) Miyamoto, A. et al.: 17th General Lecture Meeting of Kanto Branch of the Japan Society of Mechanical Engineers. 206203 (2010)
23) Furuya, K. et al.: Collection of Preprints for 2011 Spring Academic Lecture Meeting of the Society of Automotive Engineers of Japan. 69-11, 330 (2011)
24) Koizumi, T. et al.: Dynamic & Design Conference 2008, the Japan Society of Mechanical Engineers. 456-1 (2008)
25) Yamashita, S. et al.: Outlines of Academic Lectures of the Architectural Institute of Japan. B-2, Structure II, Vibration, Nuclear Power Plants. 515 (1995)
26) Furuya, K. et al.: OPTIS 2008. 2008-11
27) Ii, Y. et al.: 18th General Lecture Meeting of Kanto Branch of the Japan Society of Mechanical Engineers. 2003 (2011)
28) Ohno, J. et al.: Mechanical-Acoustic Engineering. Morikita Publishing Co., Ltd.
29) Yamazaki, T. et al.: Collection of Papers (Volume C) of the Japan Society of Mechanical Engineers. 74 (744), 196 (2008)

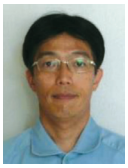

Atsushi SETO
Chief Researcher, Dr.Eng.
Forming Technologies R&D Center
Steel Research Laboratories
20-1 Shintomi, Futtsu, Chiba 293-8511

Yuichi YOSHIDA
Chief Researcher
Forming Technologies R&D Center
Steel Research Laboratories

Toyoki YAMAMOTO
Manager
Mechanical Maintenance Technology Dept.
Mechanical Engineering Div.
Plant Engineering and Facility Management Center

Shintaro KANOKO
Senior Researcher
Mechanical Engineering Div.
Plant Engineering and Facility Management Center